Pure Appl. Geophys.

DOI 10.1007/s00024-009-0004-5

Pure and Applied Geophysics

# Statistical Properties of Mine Tremor Aftershocks

T. E. Kgarume,[1,2] S. M. Spottiswoode,[1] and R. J. Durrheim[1,2]

*Abstract*—Mine tremors and their aftershocks pose a risk to mine workers in the deep gold mines of South Africa. The statistical properties of mine-tremor aftershocks were investigated as part of an endeavour to assess the hazard and manage the risk. Data from two gold mines in the Carletonville mining district were used in the analysis. Main shocks were aligned in space and time and the aftershock sequences stacked and analysed. The aftershocks were found to satisfy Gutenberg–Richter scaling, with a $b$ value close to 1. Aftershock activity diminished with time in accordance with the modified Omori law, with $p$ values close to 1. However, the relationship between the main shock and its biggest aftershock violated Båths law, with $\Delta M_L \approx 1.9$ for main shocks with $M_L < 3$ and increasing for main shocks with $M_L > 3$. The aftershock density was found to fall-off with distance as $r^{-1.3}$, suggesting triggering by dynamic stress.

**Key words:** Mine seismic events, aftershock event rate, aftershock density decay, omori's law.

## 1. Introduction

In October 2006 an incident occurred in a deep South African gold mine that motivated a renewed effort to understand the properties of mine tremor aftershocks. A $M_L = 2.4$ seismic event caused severe damage to a stope, fatally injuring several mine workers. In the investigation it was noted that an $M_L = 2.0$ event had occurred nearby 25 min prior to the $M_L = 2.4$ event, but had not caused damage to any active working places so they were not evacuated. In reviewing the incident, it was suggested that the $M_L = 2.4$ event might have been triggered by quasi-static redistribution of stress following the $M_L = 2.0$ event. The Acting Chief Inspector of Mines directed members of the "Minimising the rockburst risk" research team to investigate changes in seismic hazard following the occurrence of large seismic events, and, if warranted by the findings, to formulate guidelines regarding the evacuation of workers following such events. We report on the first phase of the investigation here—a study of the statistical properties of mine tremor aftershocks.

Local magnitude $M_L$ is used throughout this study as it is widely used to describe the size of seismic events in South African mines. Most events recorded by mine seismic networks have local magnitudes between $-1.3$ and 4.0. Mine seismic networks typically use 4.5 Hz geophones, which cannot record the low frequencies radiated by the larger events and this could lead to underestimates of the magnitudes of events with $M_L > 3$. However, the catalogue of the South African National Seismological Network (SANSN), which has a threshold sensitivity of about $M_L = 2.0$, is used to calibrate mine networks. Various methods are used to calculate $M_L$. On the mines considered in this study, a combination of energy and moment is used.

## 2. Properties of Mine Tremor Aftershocks

Mining excavations induce stresses within the surrounding rockmass, causing elastic and inelastic deformation. These stress changes can alter the stability of pre-existing zones of weakness, such as faults or the contact between dykes and the host rock. Slip may be triggered, resulting in so-called 'shear-type' events (Jager and Ryder 1999). The induced stresses are sometimes so extreme that intact rock fails, creating new shear ruptures. Seismic events

[1] CSIR, PO Box 91230, Auckland Park, Johannesburg 2006, South Africa. E-mail: rdurrhei@csir.co.za

[2] University of the Witwatersrand, Private Bag 3, Wits 2050, South Africa.

Published online: 22 December 2009

may cause rock to be ejected or shaken loose from the hanging- and sidewalls, posing a danger to mine workers, damaging infrastructure, and hindering production. Seismic events are often followed by aftershocks, which are generally considered to be triggered by quasi-static stress transfer (Shcherbakov *et al.*, 2005). These aftershocks may also pose a hazard to mining personnel and underground infrastructure, as past experience has shown that events as small as $M_L = 0.5$ can cause injuries.

The four empirical relations used in this study to analyse the properties of aftershocks are briefly described below.

### 2.1. *Gutenberg–Richter Frequency–Magnitude Scaling*

$$\log N = a - bM, \tag{1}$$

where $N$ is the cumulative number of events greater than or equal to magnitude $M$, and $a$ and $b$ are constants. The constant $a$ is a measure of the level of seismicity and gives the logarithm of the number of events with magnitudes greater than zero in the specified region and time window. The "$b$ value" is an indication of the ratio of large to small events. For global earthquakes, it is generally in the range $0.8 < b < 1.2$ (Frohlich and Davis 1993).

In the case of mining-related tremors, the $b$ value may vary from $0.5 < b < 1.5$, depending on the mining geometry. It has been suggested that the $b$ value is a function of the type, or "fractal dimension" ($D = 2b$) of the source region (Turcotte *et al.*, 2000). The dimensionality can be interpreted in terms of the shape and dimensions of the mining excavations, interactions with nearby faults and dykes that may be the locus of seismic activity, and the spacing of shear zones that may limit the size of the blocks in which strain energy is stored (Legge and Spottiswoode, 1987).

1. If $b = 0.5$, $D = 1$ and planar seismic source zones with $L$(length) $\gg$ $W$(width) are indicated. This situation arises when there is extensive mining parallel to a fault or dyke. The excess shear stress lobes produced by the excavations extend for hundreds of metres in the strike direction of the fault or dyke ($L$), but only for tens of metres in the dip-direction ($W$).
2. If $b = 1$, $D = 2$ and planar seismic source zones with $L \approx W$ are indicated. This situation arises where the source dimension parallel to the mining face ($L$) is limited to tens of metres by the leads and lags between adjacent panels.
3. If $b = 1.5$, $D = 3$ and volumetrically distributed sources are indicated with $L \approx W \approx S$, where $S$ is the shear-zone spacing. In practical terms, this means that the volume of rock contributing to each event is further limited by the presence of shear zones.

Frequency–magnitude statistics for mine tremors are often bi-modal, indicating that more than one population of events is involved. Ebrahim-Trollope (2001) reports that most events with $M_L < 0$ are a result of the fracturing of the solid rock mass after blasting. This population has a much higher $b$ value than the events generated by local structural failure, e.g., slip along faults and dykes. Richardson and Jordan (2002) identified two main classes of events: "Type A" events that are tightly clustered in time and space and generally within 100 m of an active mining face, associated with tensile fracturing and/or blasting close to the mine openings, and with an upper moment-magnitude cut-off at $M \approx 1.0$; and "Type B" events that are distributed in space and time throughout the mining region, have a distinct lower moment-magnitude cut-off at $M \approx 0.0$, and are interpreted to be due to "friction-dominated" rupture occurring on existing faults or other weak geological structures at near-lithostatic normal stresses. Spottiswoode and Linzer (2004) contested this interpretation, arguing that most, if not all, "Type A" events are actually development blasts and that the lower magnitude cut-off of "Type B" events can be explained by the triggering logic of the seismic system.

### 2.2. *Modified Omori Law*

$$n(t) = \frac{K}{(t+c)^p}, \tag{2}$$

where $t$ is the time after the main shock, $n(t)$ is the number of events occurring at time $t$, $K$ and $c$ are

parameters and $p$ is a rate constant of aftershock decay (Nanjo *et al.*, 1998). Spottiswoode (2000) studied the aftershock and foreshock time sequences of blasts and seismic events from four mines, and found them to follow Omori's law with $0.6 < p < 1.03$.

### 2.3. Båth's Law

$$\Delta M = M_{\mathrm{L}} - M_{\mathrm{as}}^{\max} \approx \text{constant}, \tag{3}$$

where $M_{\mathrm{L}}$ is the magnitude of the main shock and $M_{\mathrm{as}}^{\max}$ is the magnitude of the largest aftershock (Båth 1965). Båth's law states that the difference in magnitude between the main shock and its largest aftershock ($\Delta M$) is a constant independent of the magnitude of the main shock. For earthquakes $\Delta M$ typically has a value of about 1.2 (Båth 1965; Shcherbakov *et al.*, 2006).

### 2.4. Aftershock Density

$$\rho(r) = \frac{A}{r^n}, \tag{4}$$

where $r$ is the distance from the main shock epicentre, $\rho(r)$ is the number of events occurring at distance $r$, $A$ is a constant that varies with the number of aftershocks, and $n$ is a rate constant of aftershock decay (Felzer and Brodsky 2006). The rate of decay of the aftershock density with distance from the main shock is an indicator of the stress transfer mechanism: dynamic stresses induced by the passing seismic wave fall-off as $r^{-1.3}$, while quasi-static stresses fall-off as $r^{-3}$.

## 3. Statistical Analysis of Mine Tremor Aftershocks

The aftershock sequences were analysed following 342 $M_{\mathrm{L}} \geq 2$ main shocks at two gold mines in the Carletonville mining district exploiting the Ventersdorp Contact Reef and Carbon Leader Reef at depths of 2,500–3,500 m (note that the term "reef" denotes a quartz pebble conglomerate). Two difficulties had first to be addressed: (1) the influence of blasting during the normal mining production cycle on seismicity, and (2) the small number of aftershocks recorded after any single main shock.

### 3.1. Influence of Production Blasting on Seismicity

Mines are evacuated during blasting time and for several hours thereafter to avoid exposing workers to the hazards posed by the fumes and dust produced by the explosives and the seismicity triggered by stress redistribution following the advance of the mining face. Adjacent mines usually coordinate blasting to prevent seismicity triggered by blasting on one mine exposing workers in the adjacent mine to undue risk.

Figure 1 shows the distribution of aftershocks by hour of day for the two mines considered in this study.

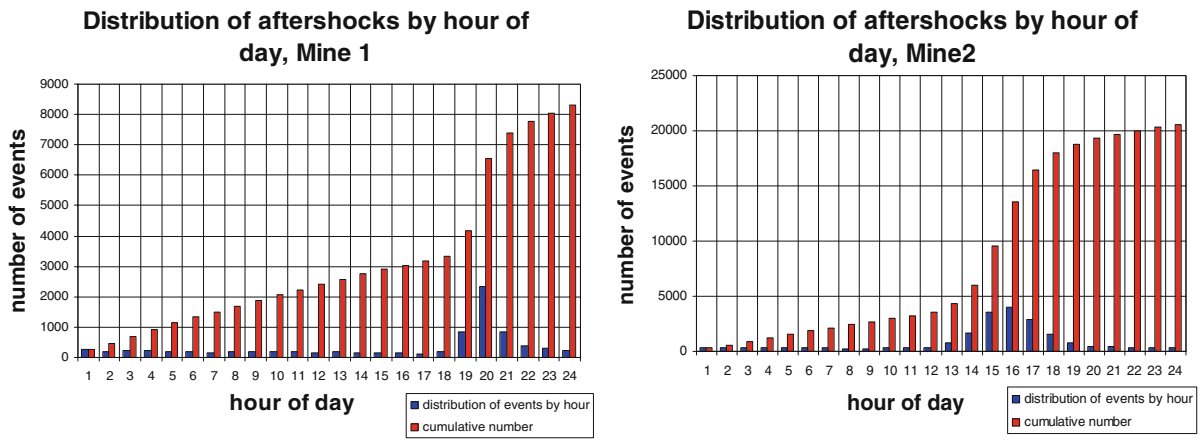


Figure 1
Distribution of $M_{\mathrm{L}} \geq 0.0$ aftershocks by hour of day within 1,000 m of the main shock epicentre. Bins are referenced to the start of each hour, e.g., bin 1 contains the number of events between 00:00:00 and 01:00:00

The number of events classified as aftershocks increases significantly at the onset of blasting time (18h00 at Mine 1 and at 12h00 at Mine 2). Smaller events ($M_L < 0.5$) occur more commonly during blasting time, while the larger events are distributed throughout the 24-h cycle. Main shocks occurring during the blasting period or in the period 4 h prior to the onset of blasting were excluded from the analysis to avoid contamination of the aftershock sequence by the flurry of seismicity triggered by normal production blasting.

### 3.2. Stacking of Aftershock Sequences

Although larger seismic events in deep-level mines are often followed by an increased rate of seismicity, the number of aftershocks following any single main shock is quite small. Typically there are fewer than five aftershocks of $M_L > 0$ for each $M_L > 2.5$ main shock, which are too few for reliable statistical analysis of event rate decay or frequency–magnitude relationships. This difficulty was overcome by stacking many main-shock–aftershock sequences, using the origin time and epicentre of the main shock as a reference (Fig. 2).

Before routinely implementing the stacking procedure, we first checked whether the aftershock generation process had any dependency on mining conditions. We investigated this by classifying the main shocks into categories based on the calculated strain rate and stress, and the proximity to dykes and faults. We then compared the aftershock productivity in areas with contrasting characteristics: (1) high and low strain rates, (2) high and low stresses, and (3) near to, or distant from, faults and dykes. No significant variation in aftershock productivity was found.

Bin sizes were adjusted to ensure that each bin contained approximately the same number of events. Consequently the bin size grew as the time after the main shock increased, or the distance from the epicentre increased. The aftershock rate was then calculated as a function of time after the main shock and as a function of the distance from the main shock epicentre.

### 3.3. Analysis Procedure

The following steps were followed to analyse the data:

1. The catalogue consisted of almost 31,000 events (see Table 1). All events with $M_L \geq 2$ were classified as "main shocks" with the exception of those that occurred within the blasting period or

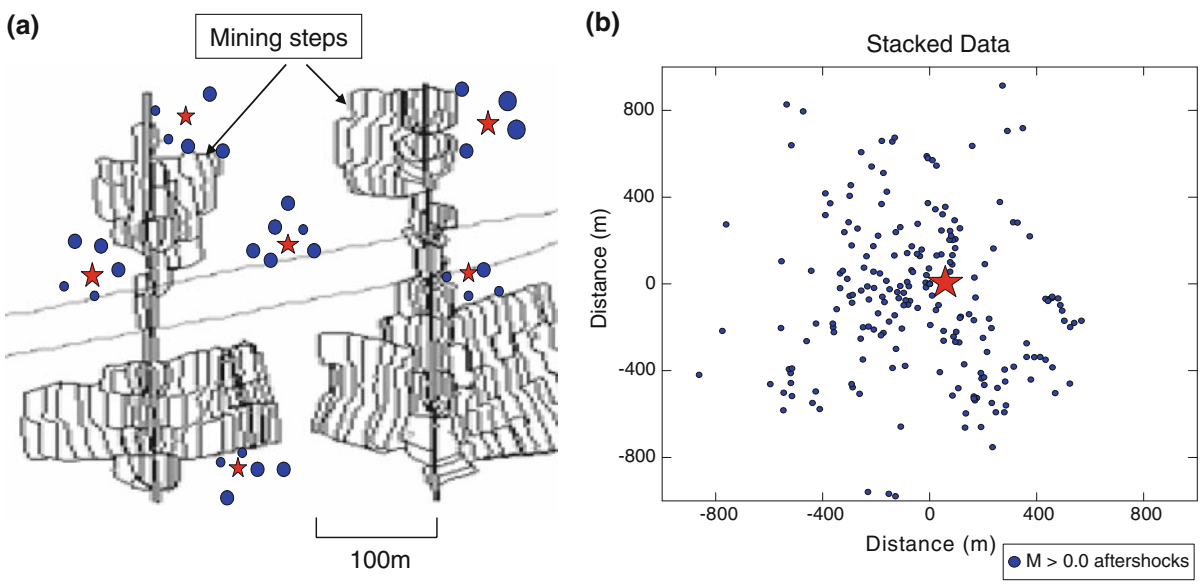


Figure 2
Stacking of different main-shock–aftershock sequences. **a** Cartoon showing a plan view of a mine with several main-shocks and aftershock clusters. The *bands* represent the position of the stope face at monthly intervals. **b** Data stacked at the origin in space

Table 1

*Mine seismicity data sets*

| | $M_L$ range | Mine 1 | | Mine 2 | |
|---|---|---|---|---|---|
| Orebody (Reef) | | Ventersdorp Contact | | Carbon Leader | |
| Start catalogue: | | 2003/01/01 | | 1998/01/02 | |
| End catalogue: | | 2007/11/09 | | 2007/01/08 | |
| Blasting time: | | 17h00–21h00 | | 12h00–18h00 | |
| No. events in catalogue | $-1 \le M_L < 4$ | 10,203 | | 20,611 | |
| Main shocks | $1 \le M_L < 2$ | 693 | | 1,184 | |
| | $2 \le M_L < 3$ | 72 | | 247 | |
| | $3 \le M_L < 4$ | 8 | | 15 | |
| Including/excluding blasting time | | Including | Excluding | Including | Excluding |
| Aftershock analysis 1 | | | | | |
| Main shocks | $2 \le M_L$ | 80 | | 262 | |
| Aftershocks: occurring prior to next main shock or within 24 h | $0 \le M_L < 1$ | 449 | 300 | 1,349 | 498 |
| | $1 \le M_L < 2$ | 110 | 63 | 443 | 171 |
| | $2 \le M_L < 3$ | 70 | 5 | 63 | 34 |
| | $3 \le M_L$ | 3 | 3 | 8 | 4 |
| Aftershock analysis 2 | | | | | |
| Main shocks | $1 \le M_L < 2$ | 693 | | 1,184 | |
| Aftershocks: occurring prior to next $1 \le M_L$ main shock or within 4 h | $0 \le M_L < M_{ms}$ | 449 | 70 | 1,349 | 498 |
| Aftershock analysis 3 | | | | | |
| Main shocks | $2 \le M_L < 3$ | 72 | | 247 | |
| Aftershocks: occurring prior to next $2 \le M_L$ main shock or within 5 h | $0 \le M_L < M_{ms}$ | 163 | 143 | 350 | 206 |
| Aftershock analysis 4 | | | | | |
| Main shocks | $3 \le M_L < 4$ | 8 | | 15 | |
| Aftershocks: occurring prior to next $3 \le M_L$ main shock or within 11 h | $0 \le M_L < M_{ms}$ | 61 | 51 | 103 | 62 |

All main shocks occurring during blasting time were excluded. Aftershocks were defined as any $M_L \ge 0$ event that occurred within 1,000 m of the main-shock epicentre event during the specified time window

in the four hours prior to the blasting period. These were excluded from the analysis to avoid contaminating the aftershock sequences with the many small events that are triggered by blasting.

2. Events with magnitude $0 \le M_L < M_{ms}$ occurring within 1,000 m of the main-shock epicenter and prior to the next main shock or within 24 h of the main shock were classified as "aftershocks." Although there undoubtedly are aftershocks with $M_L < 0$, only aftershocks with $M_L \ge 0$ were considered in this study, as smaller events do not pose a significant risk. The aftershock sequences were aligned in space and time.
3. Aftershock sequences were binned and stacked to determine the rate of decay of aftershocks as a function of time and distance. Gutenberg–Richter, modified Omori, Båth's law and aftershock density analyses were conducted for various main-shock and aftershock thresholds. The details of each analysis are described in the respective sections below.

## 4. Findings

As the results for Mine 1 (Ventersdorp Contact Reef) and Mine 2 (Carbon Leader Reef) are similar, in most cases only one example is shown.

### 4.1. Gutenberg–Richter Frequency–Magnitude Scaling

The frequency–magnitude statistics for $M_L \ge 0$ events that occurred within 1 h and 1,000 m of $M_L \ge 2$ main shocks were compared with a data set comprised of nearly 3,000 $M_L \ge 0$ seismic events that occurred more than 6 h after an $M_L \ge 2$ main shock. The latter data set were considered unlikely to

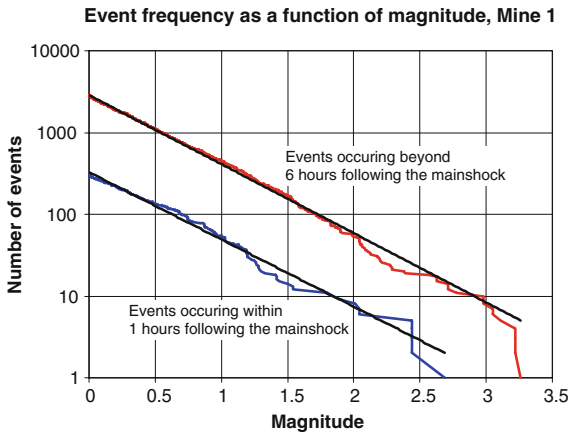


Figure 3
Gutenberg–Richter frequency–magnitude relation for potential aftershocks and background seismicity

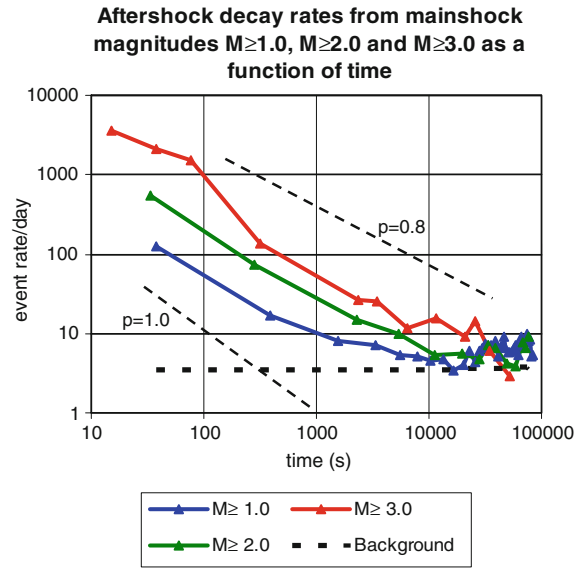


Figure 4
Investigation of the modified Omori law, showing aftershock activity as a function of main shock magnitude. The $p$ value was estimated within the interval 15 s $\leq t \leq$ 83365 s

be aftershocks and taken to represent background seismicity (Fig. 3). Both the aftershock and background frequency–magnitude data are uni-modal and the $b$ values are virtually identical with $b = 0.8$.

### 4.2. *Modified Omori Analysis*

The decay in the rate of aftershocks with time for three main shock thresholds ($M_L = 1$, 2 and 3) is shown in Fig. 4. The following procedure was used to analyse the data:

1. All events with magnitudes greater than the particular main shock threshold $M_L$ were selected and designated as main shocks. The aftershock sequences corresponding to each main shock threshold were selected. The lower threshold for aftershocks was $M_L = 0$.
2. Bin sizes were adjusted to ensure that each bin contained the same number of events (20 events per bin for Mine 1, 40 events per bin for Mine 2).
3. The event rate for each bin was calculated (expressed in events/day) and plotted at the average time of the events within the bin. The bin size has no effect on the event rate as it is taken into account in the calculation.
4. A curve was fitted to the data to determine the parameters of the modified Omori model.

While larger main shocks were more productive in terms of the number of seismic events, all subsets

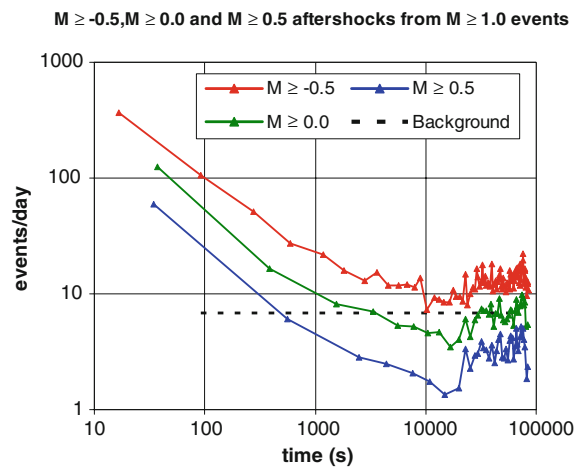


Figure 5
Investigation of the modified Omori law, showing aftershock activity for various lower aftershock threshold magnitudes. The $p$ value was estimated within the interval 16 s $\leq t \leq$ 84407 s

yielded $p$ values in the range $0.8 < p < 1.0$ (Fig. 4). The lower aftershock threshold magnitude (Fig. 5) and the radius of the 'zone of influence' (Fig. 6) had a negligible effect on the calculated $p$ values. Few aftershocks were recorded at distances greater than 300 m from the main shock.

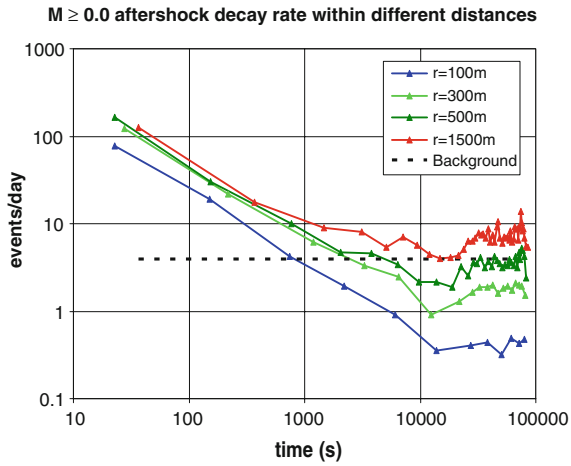


Figure 6
Investigation of the modified Omori law, showing aftershock activity as a function of distance from the main-shock epicentre

The 'time offset' parameter was in the range $1\text{ s} < c < 20\text{ s}$ (Fig. 7). The $c$ value was found to increase with increasing main shock magnitude, as has been found for tectonic earthquakes (SHCHERBAKOV *et al.*, 2004). It was inversely related to the maximum aftershock magnitude. The $c$ value is interpreted to be an artefact of the system-triggering logic. It is likely that some aftershocks (especially the smaller ones) that occur soon after a main shock are lost owing to automatic adjustments in the data-adaptive triggering algorithm.

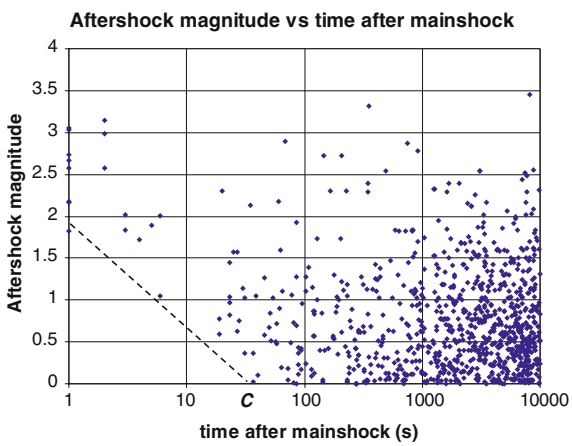


Figure 7
Investigation of the modified Omori law, showing the time offset parameter

### 4.3. *Båth's Law*

The magnitude of the biggest mine tremor aftershock was found to be, on average, 1.9 magnitude units less than the main shock magnitude (Fig. 8). This difference increases as the main-shock magnitude increases above 3.0. We believe that this is due to the fact that the maximum magnitude of mining-related tremors is controlled by the mining span. The largest events occur when the entire zone subjected to excess shear stress (ESS) experiences slip, leaving relatively little residual ESS to be released in aftershocks.

### 4.4. *Aftershock Density*

The aftershock density fall-off rate is a parameter that may be used to distinguish between different aftershock triggering mechanisms. The procedure

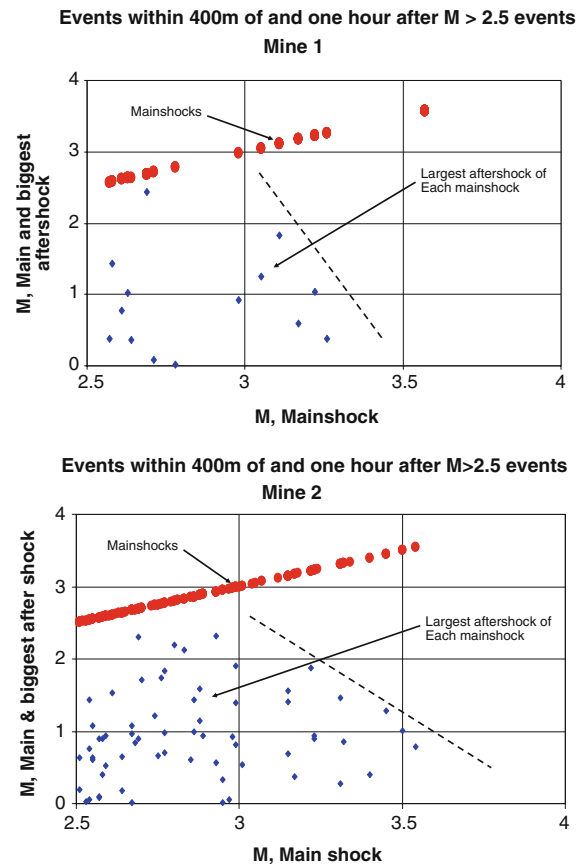


Figure 8
Investigation of Båth's law

used to calculate the fall-off rate is illustrated by means of the example shown in Fig. 9. It should be noted that the data are normalised to the number of events in the outermost zone to facilitate the display. Our primary interest is in the change of density with distance (i.e., the fall off rate) and not the absolute value of the aftershock density.

1. Aftershocks following 246 main shocks and $2 \leq M_L < 3$ main shocks on the Carbon Leader Reef mine occurring within 2 h or prior to the next $2 \leq M_L$ main shock, whichever is less, were analysed. The main-shock and aftershock locations were projected onto the reef plane. We do this because (1) most mine tremors are located close to the reef plane as this is where the mining-induced stress and the strain-energy release is greatest, and (2) the coplanar configuration of the seismic network means that the on-reef location errors are considerably less than the errors perpendicular to the reef.
2. Aftershock sequences were aligned in space and time. The aftershocks were sorted into seven concentric zones with outer radii of 50, 100, 150, 200, 300, 500 and 1,000 m. The radii of the zones were chosen to give approximately equal numbers of aftershocks in each zone. The number of aftershocks in each zone was summed and normalised by the number of events occurring in the outermost zone (500–1,000 m). While the number of events in each zone (red diamonds in Fig. 9) is roughly the same, it should be noted that the density of aftershocks decreases with distance, as the area of each zone increases with distance from the epicentre.
3. The background seismic activity was calculated by considering the number of events within 1,000 m of the actual location of each main shock during a 7 day period of normal mining activity. The background events were aligned in space and time and sorted into zones with the same radii as were used to bin the aftershocks. The number of events in each zone was summed and normalised by the number of events in the outermost zone (blue squares in Fig. 9). The number of events in the outermost zone (500–1,000 m) is roughly ten times greater than the number in the innermost zone (radius 50 m), while its area is about 300 times greater. This is because the background seismicity is not randomly distributed in space, but tends to cluster near mining excavations.
4. The rate at which the density of aftershocks falls off with distance was determined by calculating the ratio of the normalised number of aftershocks to a model of the background seismicity. Two different numerical models were used to explain the background seismicity (Spottiswoode *et al.*, 2008).

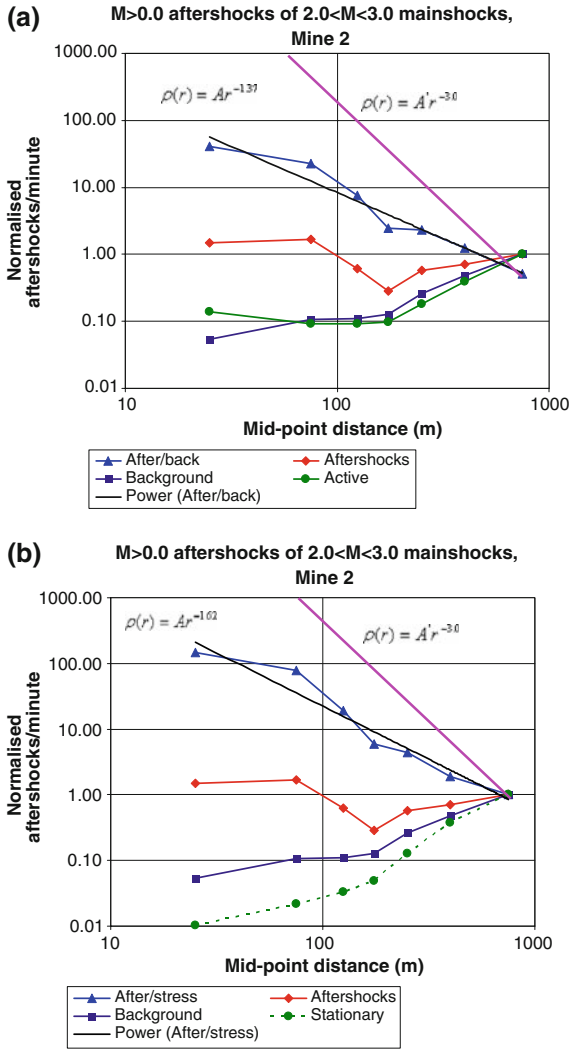


Figure 9
Investigation of the aftershock density as a function of distance from the main shock. The background seismicity is modelled as a function of (**a**) energy release rate or "active mining" and (**b**) stress or "stationary mining." Details of the analysis are given in the text

(a) The "active" model considers the strain energy released by active mining to be the principal driver of both main- and aftershocks. An area is defined as "active" if mining took place in the month prior to the main shock. The normalised number of events in each zone predicted by this model is remarkably similar to the observed background seismicity (green circles and blue squares in Fig. 9a, respectively). A curve (black line in Fig. 9a) was fitted to the aftershock/background ratio (blue triangles in Fig. 9a), showing a constant fall-off as $r^{-1.37}$. Also shown in Fig. 9a is a line showing the fall-off of aftershock density as $r^{-3}$, which would have been followed if the triggering was due to quasi-static stresses.

(b) The "stationary" model considers the possibility that aftershocks may also be triggered in the stressed ground around old mining faces. On-reef stress in excess of 300 MPa was considered to be sufficiently high for the rock to be in a state of incipient failure. The normalised number of events in each zone predicted by this model is considerably smaller than the observed background seismicity (green circles and blue squares in Fig. 9b, respectively). A curve (black line in Fig. 9b) was fitted to the aftershock/"stationary" ratio (blue triangles in Fig. 9b). A fit to the data shows a constant fall-off as $r^{-1.62}$.

Felzer and Brodsky (2006) found that that the density of earthquake aftershocks falls off with the distance from the main shock as $r^{-1.3}$, which is comparable to the decay of the maximum seismic wave amplitude (a proxy for dynamic stresses). We obtain a similar fall-off rate for mine tremors. Therefore our analysis, like that of Felzer and Brodsky (2006), supports the view that most aftershocks are triggered by dynamic stresses (which is proportional to the amplitude of radiated seismic wave) rather than by quasi-static stress redistribution, even though many aftershocks do not occur at the time when the shaking occurs. Furthermore, it supports the conclusion by Spottiswoode *et al.*, (2008) that seismicity is driven primarily by the strain energy changes due to active mining, rather than by high stresses, which are found in both areas of active and past mining.

## 5. *Hazard Associated with Aftershocks*

The ultimate objective of this investigation is to provide guidelines governing: (1) the evacuation of workers following a main shock during a working shift, and (2) the entry of workers following a main shock during blasting time. The procedures described above can be used to determine objectively and quantitatively the period following a large seismic event during which people should be excluded from working areas.

Our results and those of Spottiswoode (2000) demonstrate that the modified Omori model is applicable to mine seismic data and can be used to estimate the hazard posed by aftershocks. It is evident that the probability of a seismic event with the potential to cause injury increases significantly immediately after a moderate-sized event, say $M_L > 2$. The number of aftershocks falls off with time, reaching background levels after 4–10 h, depending on the main-shock magnitude.

Guidelines for the evacuation of and/or re-entry to working places are summarized in Table 2. The time periods for which the aftershock event rate has reached 10× and 3× the background rate were determined from the Omori decay curve of

Table 2

*Time period for the aftershock event rate to reach 10× and 3× the background rate*

| $M_{main\ shock}$ | 10× (mins) | | 3× (mins) | |
|---|---|---|---|---|
| | 0–200 m | 200–400 m | 0–200 m | 200–400 m |
| Mine 1: VCR mine | | | | |
| $1 \le M_L < 2$ | 5 | 2 | 24 | 30 |
| $2 \le M_L < 3$ | 16 | 5 | 180 | 162 |
| $3 \le M_L < 4$ | 48 | 60 | 300 | (480) |
| Mine 2: CLR mine | | | | |
| $1 \le M_L < 2$ | 3 | 2 | 16 | (78) |
| $2 \le M_L < 3$ | 10 | 3 | 48 | 15 |
| $3 \le M_L < 4$ | 60 | 24 | 120 | (120) |

Time is given in minutes and distance in meters from the main-shock epicentre. The times given in brackets are subject to considerable uncertainty owing to a small number of events

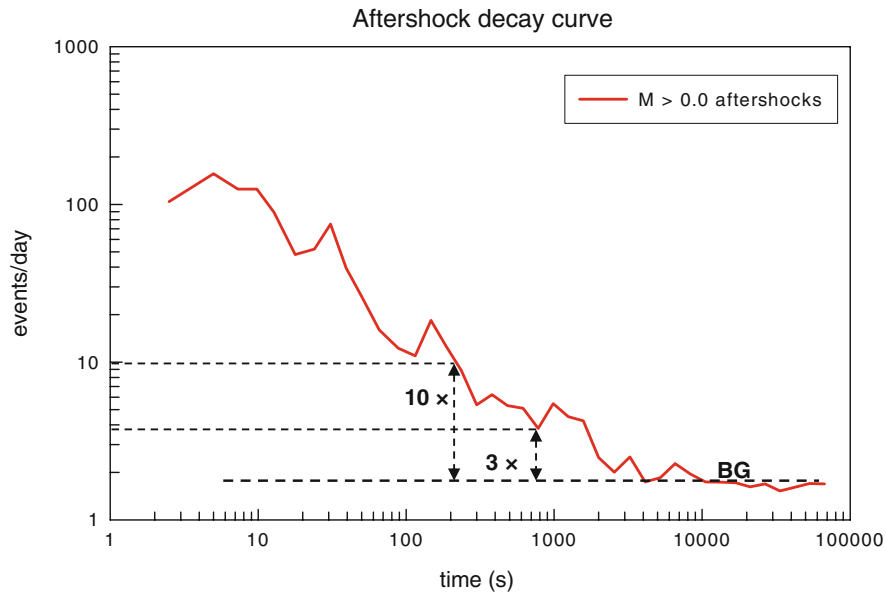


Figure 10
Use of the Omori decay curve to determine the time taken for seismic hazard to decrease to acceptable levels. 10× and 3× represent the time taken for the aftershock rate to decrease to ten times and three times the background rate

aftershocks (Fig. 10). As an example, in case of an occurrence of a $3.0 \leq M_L < 4.0$ main shock at the VCR mine, it takes about 48 min for aftershock activity to decreased to 10× the background level.

## 6. Conclusions

Aftershocks of tremors occurring in two deep gold mines in the Carletonville area were found to satisfy Gutenberg–Richter scaling with a $b$ value close to 1. Aftershock activity diminished with time in accord with the modified Omori law, with $p$ values close to 1. However, the difference between the magnitude of the main shock and its biggest aftershock was not in accordance with Båths law for earthquakes. The difference was to average 1.9 and increasing for main shocks with $M_L > 3$. The aftershock density was found to fall-off with distance as $r^{-1.3}$, suggesting triggering by dynamic stresses and not simply quasi-static stress changes.

The procedures described here can be applied to different mines, and used to determine the period for which people should be excluded from working areas should a large seismic event occur. The period for which exposure should be reduced depends on the level of risk that is considered to be tolerable. The definition of "acceptable risk" is a necessary and significant consideration in any mining project or operation and is inextricably linked to ethics. This requires input from executive management, government, labour, and civil society

## Acknowledgments

This study forms part of project SIM 050302 "Minimising the rockburst risk" sponsored by the Mine Health and Safety Council (MHSC). Mine management is thanked for providing the seismic data.

## References

Båth, M. (1965), *Lateral inhomogeneities in the upper mantle*, Tectonophysics *2*, 483–514.

Ebrahim-Trollope, R. (2001), *Gutenberg–Richter relationship and mine-induced seismicity as observed at the African Rainbow Minerals mines—Klerksdorp*, *Proc. Fifth Int. Symp. Rockbursts and Seismicity in Mines* (Van Aswegen, G., Durrheim, R.J., and Ortlepp, W.D., eds), The South African Institute of Mining and Metallurgy, Symposium Series *S27*, pp. 501–508.

Felzer, K.R. and Brodsky, E.E. (2006), *Decay of aftershock density with distance indicates triggering by dynamic stresses*, Nature *441*(8), 735–738.

FROHLICH, C. and DAVIS, S.D. (1993), *Teleseismic b values—or, much ado about 1.0*, J. Geophys. Res. *98*. B1, 631–644.

JAGER, A.J. and RYDER, J.A., *A Handbook on Rock Engineering Practice for Tabular Hard Rock Mines* (SIMRAC, Johannesburg, 1999).

LEGGE, N. and SPOTTISWOODE, S.M. (1987), *Fracturing and microseismicity ahead of a deep gold mine stope in the pre-remnant and remnant stages of mining*. *Proc. Sixth Congress of the Int. Soc. Rock Mechanics* (G. Herget and S. Vongpaisal, eds) (A. A. Balkema, Rotterdam, The Netherlands, 1987) pp. 1071–1077.

NANJO, K., NAGAHAMA, H., and SATOMURA, M. (1998), *Rates of aftershock decay and the fractal structure of active fault systems*, Tectonophysics *287*, 173–186.

RICHARDSON, E. and JORDAN, T.H. (2002), *Seismicity in deep gold mines of South Africa: implications for tectonic earthquakes*. Bull. Seismol. Soc. Am. *92*, 1766–1782.

SHCHERBAKOV, R., TURCOTTE, D.L., and RUNDLE, J.B. (2005), *Aftershock statistics*, Pure Appl. Geophys. *165*, 1051–1076.

SHCHERBAKOV, R., TURCOTTE, D.L., and RUNDLE, J.B. (2004), *A generalized Omori's law for earthquake aftershock decay*, Geophys. Res. Lett. *31*, L11613, doi:10.1029/2004GL019808.

SHCHERBAKOV, R., TURCOTTE, D.L., and RUNDLE, J.B. (2006), *Scaling properties of the Parkfield aftershock sequence*, Bull. Seismol. Soc. Am. *96*, S376–S384.

SPOTTISWOODE, S.M. (2000), *Aftershocks and foreshocks of mine seismic events*, *Proc. Third Int. Workshop on the Application of Geophysics to Rock and Soil Eng.*, Melbourne, Australia, November 2000.

SPOTTISWOODE, S.M. and LINZER, L.M. (2004), *Improved seismic locations and location techniques*, SIM 020304 Final Project Report (Appendix 1), Mine Health and Safety Council, Johannesburg, South Africa.

SPOTTISWOODE, S.M., LINZER, L.M., and MAJIET, S. (2008), *Energy and stiffness of mine models and seismicity*. In *SHIRMS 2008* (Y. Potvin, J. Carter, A. Dyskin, R. Jeffrey, eds), Australian Centre for Geomechanics, Perth, Australia, vol. 1, pp. 693–707.

TURCOTTE, D.L., NEWMAN, W.I., and GABRIELOV, A. (2000), *A statistical physics approach to earthquakes*. In *Geocomplexity and the Physics of Earthquakes* (J.B. Rundel, D.L. Turcotte and W. Klein, eds), Geophysical Monograph *120*, American Geophysical Union, Washington, DC, U.S.A., pp. 83–96.

(Received September 26, 2008, revised April 9, 2009, accepted April 21, 2009)